NGU REPORT 2021.004

Acquisition, processing and interpretation of snow-streamer seismic profiles in Masi and Sennalandet, Finnmark, northern Norway

GEOLOGY FOR SOCIETY

SINCE 1858

GEOLOGICAL SURVEY OF NORWAY

- NGU -

NORGES GEOLOGISKE UNDERSØKELSE
- NGU -

REPORT

Geological Survey of Norway
P.O.Box 6315 TORGARDEN
NO-7491 TRONDHEIM
Tel.: 47 73 90 40 00

Report no.: 2021.004

ISSN: 0800-3416 (print)
ISSN: 2387-3515 (online)

Grading: Open

Title: Acquisition, processing and interpretation of snow-streamer seismic profiles in Masi and Sennalandet, Finnmark, northern Norway

Authors:
Bent Ole Ruud, Odleiv Olesen, Jomar Gellein & Tor Arne Johansen

Client:
NGU

County:
Troms og Finnmark

Municipality:
Kautokeino, Hammerfest

Map-sheet name (M=1:250.000)
Nordreisa and Hammerfest

Map-sheet no. and -name (M=1:50.000)
1833 I, 1933 IV, 1935 II, 2935 III, 1935 IV

Deposit name and grid-reference:

Number of pages: 35 **Price (NOK):** 130
Map enclosures:

Fieldwork carried out:	**Date of report:**	**Project no.:**	**Person responsible:**
March-April 2012	13.02.21	3471.00	Hanco Brönner

Summary:
Two snow-streamer profiles were acquired by the University of Bergen in March and April 2012 within the programme 'Mineral Resources in Northern Norway - MINN'. The two profiles are located in the Masi and Sennlandet areas in the Kautokeino and Hammerfest municipalities. The data were acquired using a combination of snow-streamer and autonomous nodes. The obtained reflectors can be traced to a depth of 4-5 km. P-wave velocities are obtained from travel-time tomography of manually picked first breaks. The velocities can be resolved down to a few hundred meters depth.

We have included two interpretation examples of the Masi profile in the current acquisition and processing report. The regional c. 4-5 km wide Mierojávri-Sværholt shear zone is represented by several reflectors dipping at an angle of c. 40-50° to the southeast below the northwestern margin of the Jergul Gneiss Complex. The migrated seismic profile shows that the dip of the western and eastern segments of the Masi fault system (within the Stuoragurra fault complex) is 52° and 65°, respectively. The two postglacial fault segments seem to merge at a depth of c. 500 m.

The present study proves that snow-streamer technology is an efficient way to carry out seismic profiling in snow-covered and relatively flat terrain. Using detonating cord as a seismic source has left no permanent footprint on the sparse vegetation in the Arctic, which is an advantage. We conclude that the reflection seismic data are of high quality and that the obtained reflectors can be interpreted in terms of regional geological structures continuing to a depth of 3-4 km. We suggest that the western part of the reprocessed Masi profile, and the Sennalandet profile, should be interpreted in a similar integrated way as the examples shown in the present report.

Keywords:	Geophysics	Geology
Seismic method	Processing	Interpretation
		Report

CONTENTS

1. INTRODUCTION

In 2011 NGU received government funds to acquire geophysical data from northern Norway. Two snow-streamer profiles were acquired in 2012 within the programme 'Mineral Resources in Northern Norway - MINN'. The two profiles are located in the Masi and Sennalandet areas in the Kautokeino and Hammerfest municipalities (Figures 1A & 5).

Table 1. Profile coordinates, WGS84 zone 33

Masi east	840418 E	7730745 N	850140 E	7727539 N
Masi central	839235 E	7730783 N	835385 E	7733114 N
Masi west 1st section	835385 E	7733114 N	830620 E	7730673 N
Masi west 2nd section	830620 E	7730673 N	828677 E	7729443 N
Masi west 3rd section	828677 E	7729443 N	828000 E	7728849 N
Sennalandet east	844759 E	7819351 N	849679 E	7815637 N
Sennalandet west	841780 E	7821032 N	830859 E	7830825 N

2. DATA ACQUISITION

Seismic data were acquired by the University of Bergen during March and April 2012. The data were acquired using a combination of snow-streamer and autonomous nodes. The snow-streamer technology (Eiken et al., 1989; Johansen et al, 2011) is an efficient way to do seismic profiling in snow-covered and relatively flat terrain. The seismic source used is detonating cord which, besides being very efficient and producing favourable source directivity, advantageously leaves no permanent footprint into the ground. Two parallel detonating cords separated by 1 m were deployed in intervals of 50 m (Figure 1, bottom pictures). Each sensor of the snow-streamer consisted of eight gimballed geophones connected in strings of length 25 m, see Rygg et al. (1992) for details regarding the snow-streamer layout and operation. The seismic data were acquired with 2 ms sampling and 6 s recording time. The snow-streamer recorded 60 traces with offsets from 125 to 1625 m. Up to 40 nodes were used in addition to the snow-streamer. The purpose of the autonomous nodes was mainly to record traces with larger offsets, and to acquire data in areas with rough terrain where the snow-streamer could not be used. Two geophone strings with the same type of sensors as used for the snow-streamer were connected to each node, which recorded data from the same sources as the snow-streamer.

Three lines were shot near Masi; See map in Figure 2. The eastern line was shot first, from the west towards the east. Then the middle line was shot from the east toward the west, and finally, the eastern line was also shot from the east towards the west. The layout of shots and receivers for the eastern line is shown in Figure 3.

From this figure, we see that the first 2 km of the line is covered only by nodes, due to the steep terrain. The first shot was fired about 0.9 km from the start of the line. While shooting up to about 3.8 km the streamer lay still, and after that the streamer was operated as normal; that is, it was moved along with the shots (with a constant offset) until the end of the line. The nodes were not moved until the shots had reached about 5.0 km into the line. Thereafter, the nodes were moved two times. The lower part of Figure 3 shows the layout transformed into common mid-point (CMP) and offset. The middle line was recorded with nodes only due to hilly terrain. The nodes were laid out and moved in three batches, as shown in Figure 4. Some shot points near 3 km from the start of the line were not used since the line was crossing the Rv 93 (now E45) highway and a high voltage power line. The source and receiver layout for the western line is shown in Figure 5. Where the line was crossing over water, shots were not fired.

At Sennalandet, two lines were shot, as shown in the map of Figure 6. The western line was shot first from the east towards the west, and then the eastern line was shot from the west towards the east. The layout of sources and receivers are shown in Figures 7 and 8. The western line was crossing over several small lakes. Because no shooting was allowed at the ice-covered lakes, the shot coverage is incomplete, especially in the westernmost part. The eastern line was recorded by snow-streamer only.

3. DATA PROCESSING

The data processing started with the usual steps for seismic reflection profiling with trace editing, static corrections (including elevation), muting, amplitude corrections, surface consistent deconvolution, and various kinds of filtering and noise reduction techniques. In the noise reduction process, velocity filtering (both in the frequency-wavenumber (f-k) and intercept time-ray parameter (tau-p) domains) was used to enhance P-wave reflections while reducing surface waves, S-waves, ambient noise and incoherent energy.

After noise reduction, static corrections and a velocity model based on refracted P-waves, was determined. Due to a general lack of clear reflections, the statics were derived from first breaks following a method explained in Appendix I. Surface consistent delay times were determined for all source and receiver positions together with lateral varying velocities for refracted P-waves propagating in the shallow part of the crust (for offsets in the interval 100 – 1000 m). The purpose of including both delays and variable velocities is that the velocities should accommodate smooth velocity variations in the solid bedrocks. In contrast, the delay times should accommodate more local velocity heterogeneities, such as variations in depth to the bedrock, presence of peats or lakes etc. The obtained velocity models were used in subsequent NMO (normal move-out) and DMO (dip move-out) processing. The DMO

process used was an integral (Kirchhoff) method. After inverse NMO, the unstacked DMO corrected CMP bins were subject to a traditional reflection type velocity analysis before new NMO correction and stacking with the new velocity model. Finally, the DMO stacks were migrated and depth converted. Pre-stack Kirchhoff time migration was also tested, but since migration artefacts (due to edge effects from the many line segments and uneven offset coverage) were more severe than for DMO, the post-stack migrated DMO stacks were preferred.

Processing sequence:

- set geometry
- trace editing
- notch filter (50 Hz)
- mute (external)
- bandpass filter (10-20-100-125 Hz)
- amplitude recovery
- incoherent noise attenuation (FX projection)
- surface consistent deconvolution (spiking)
- fk-filtering (remove low velocity waves < 3500 m/s)
- mute (internal to remove air waves)
- high-resolution velocity filtering (tau-p domain)
- static corrections
- CMP sorting
- NMO correction
- DMO corrections
- inverse NMO correction
- velocity analysis
- NMO corrections (with new velocity model)
- elevation statics (datum 500m asl)
- stacking
- migration (FD)
- depth conversion

4. SEISMIC TOMOGRAPHY

The velocity model obtained from the static estimation gives information about lateral velocity variation only: there was no information about the vertical variations. If the velocity increases with depth, which is usually the case, the refracted arrivals (for sufficiently larger offsets) can be used in a tomographic inversion to estimate a 2D velocity model. Due to the low signal to noise ratio at large offsets, the first arrivals were picked manually for the tomographic inversion. The manually picked arrivals are more reliable than auto picks. However, due to the large amount of traces, the picking could not be done for every trace, so the resolution is less than for the auto picking. A free software package for 2D seismic tomography, developed by Korenaga et al. (2000), was used to invert first arrivals up to an offset of 5 km. No layering or

reflectors were defined in the initial model, so the velocities are assumed to be smooth and increasing with depth. Unfortunately, the first arrivals do not indicate that the velocities increase much with depth. Thus, the rays will not dive very deep into the crust so that velocities can only be resolved down to a few hundred meters. To handle/reduce the problem caused by the low-velocity gradient, the inversion was carried out in several stages, starting with the smallest offsets and gradually increasing the offset range. The starting model had a constant velocity gradient, with a velocity of 5.0 km/s at the surface and 6.0 km/s at 1.0 km depth.

5. RESULTS

5.1 First break analysis

Masi lines: The automatically picked first breaks are shown in the upper parts of Figures 9, 10 and 11, while the derived velocity models and delay times are shown in the lower parts of the same figures. Obviously, the auto picks are very scattered, but due to a robust inversion method, the obtained velocity models are seen to resemble the trends in the auto picks quite well. For the eastern line (Figure 9), we note large delay times and low velocities near the western end of the line (0.5-1.0 km). The velocity of dry (above the water table) and unconsolidated sand/gravel may be very low suggesting a sizable depth to the bedrock in this area. For the middle line, we note the very low velocity (c. 3.5 km/s) about 1.3 km from the eastern end of the line, which seems to coincide with the Stuoragurra fault. For the western line, the velocities are often significantly higher than for the two other lines, but we note two points near 0.9 and 2.0 km with very significant delay times. These two points coincide with narrow ridges seen in the elevation data. The delays are too large to be explained by bedrock velocities in the ridges, indicating that the ridges contain sand/gravel.

Sennalandet lines: The western line (Figure 12) shows a remarkable drop in velocities between 1.0 and 2.0 km from the start of the line (eastern end) where the line is crossing the extension of the Repparfjorddalen. Otherwise, the velocities are quite high. The many gaps in the data are due to the numerous small lakes that the line must cross. For the eastern line (Figure 13), we note a gradual drop in velocity in the eastern direction.

5.2 Seismic sections and tomography

Masi lines: The seismic sections from these three lines were assembled (and reversed when necessary) into a (more or less) continuous profile and displayed in Figures 14 and 15. In the upper part of Figure 14, the DMO corrected stack is shown, and the lower part shows the migrated stack. The depth converted migrated stack is shown in the upper part of Figure 15, together with the tomography section below. The tomography results seem to indicate a depth resolution of maximum 0.5 km,

probably much less near the end of each line segment. Low-velocity anomalies correlated very well with low velocities in the near surface velocity model derived together with the statics. Low velocities near the surface, or large delay times (or the combination of these) derived in the static analysis, are seen to result in low velocity anomalies in the tomographic velocity model. Several steep, eastward dipping reflectors are seen between 11 and 12 km, where the profile crosses the Stuoragurra fault. These steep reflectors are clearest in the DMO stack. After migration these reflectors appear shorter (shallower), which is an expected effect of the migration. They are also not that clear, which may be a consequence of the migration operator smearing out noise in the data, partly hiding real reflectors. The western line segment seems to contain several clear reflectors with relatively low dip, which makes them more suitable for seismic reflection imaging.

Sennalandet lines: These are displayed in Figures 16 (DMO stack above, migrated stack below) and 17 (depth converted stack above, tomography velocities below). An interesting feature here is the steep westward dipping reflectors which reach the surface between 13 and 14 km. This area also contains a strong low velocity anomaly. The shape of this anomaly at depth is probably not reliably resolved since the anomaly is located close to one end of the western line where deeply diving rays, belonging to first arrivals, are unlikely to exist.

6. INTERPRETATION

We have in the current acquisition and processing report included two interpretation examples: (1) Integrated interpretation of the Masi profile using existing MT, gravity and magnetic data (Mrope et al., 2019) and (2) Seismic interpretation of the reprocessed central and eastern line of the Masi profile (Olesen et al., in press). The interpretations are taking into account pre-existing geological and geophysical data (Solli, 1988; Olesen et al., 1992; Olesen & Sandstad, 1993; Dalsegg & Olesen, 2014; Nasuti et al., 2015; Hendersom et al., 2015). Interpretation #1 is based on the original seismic processing while interpretation #2 s based on the reprocessed version. We conclude that the new seismic data are of high quality and we suggest that remaining data should also be interpreted using a similar integrated approach.

Seismic reflection profiles will mainly show contacts between layers of contrasting acoustic impedance, which is the product of seismic velocity and density. Fractures in rocks will lower the velocities so that fault zones can also sometimes be seen. To produce clear reflections, it is necessary for the interfaces to have a sufficient horizontal extent and to be relatively flat-lying. Of the rock types exposed along the Masi seismic line, amphibolite and diabase are expected to have a higher acoustic impedance than mica schist and quartzite, and contacts between those rock types may therefore generate prominent reflections.

The migrated seismic profile across the Masi area with interpretation is shown in Figure 18. The regional c. 4-5 km wide Mierojávri-Sværholt shear zone (MSSZ), shown with pale green colour in the map in Figure 20, is represented by several reflectors dipping at an angle of c. 40-50° below the northwestern margin of the Jergul Gneiss Complex (Siedlecka & Roberts, 1996; Olesen & Sandstad, 1993). Olesen et al. (1992), Olesen & Sandstad (1993) and Henderson et al. (2015) interpreted a dextral displacement along the MSSZ and related the contractional Biggevárri duplex to the Paleoproterozoic deformation (Figure 20). Several hundred metres thick diabases and albite diabases (Figure 20) intruded along the MSSZ 2220 ± 7 Ma ago (Bingen et al., 2015). Some of the seismic reflectors coincide with known dykes and sills that are deformed due to later movements along the fault zone (Solli, 1988; Olesen et al., 1992). The deformation is mostly related to the Svecofennian orogeny (c. 1700-1900 Ga).

The Stuoragurra fault complex (SFC) constitutes the northernmost part of the Lapland province of postglacial faults and is located within the regional MSSZ (Olesen et al., 1992, in press; Olesen & Sandstad, 1993; Bingen et al., 2015; Henderson et al., 2015). The SFC crosscuts till, an esker and other glacifluvial deposits on Finnmarksvidda (Olesen 1988, 1992; Dehls et al., 2000; Olesen et al., in press). The Máze fault system (MFS) represents the central and youngest part (< 600 years old, Olsen et al. 2021; Olesen et al., in press) of the SFC and is located at the northwestern boundary of the MSSZ while the southern and northern parts are located in the middle of the fault zone.

The migrated seismic profile in Figure 18 shows that the dip of the western and eastern segments of the SFC/MFS (marked by red lines) is 52° and 65°, respectively. The two postglacial fault segments seem to merge at a depth of c. 500 m. An electric resistivity tomography profile (ERT) across the easternmost segment of the Máze fault system indicates a water-bearing fracture zone with a dip of c. 70° to the SE (Dalsegg & Olesen, 2014).

The flat-lying reflector (marked with a white question mark) immediately to the right of the MSSZ at a depth of c. 3.5 km in Figure 18 may represent a tectonic ramp associated with a phase of thrusting or detachment faulting along the fault zone. The flat-lying reflector can alternatively originate from a structure located out of the plane. Magnetotelluric (MT) data (Mrope et al. 2019) show that a c. 1 km wide and vertical low-resistivity zone along the postglacial faults extends to a depth of c. 1.3 km. The vertical dip of the low-resistivity zone is most likely caused by a reduced sensitivity of the MT inversion method to the dip of electrical conductors. One vertical low-resistivity zone occurs also on either side of the SFC within the MSSZ. Mrope et al. (2019) also interpreted an older processed version of the seismic line and produced a combined interpretation with the MT resistivity, magnetic and gravity modelling (Figure 19).

The regional MSSZ continues to the northeast, and faults crosscut the Cryogenian to Cambrian Dividal Group as well as the above-lying Caledonian nappes (Figure 20). A syn-sedimentary movement during the deposition of the Dividal Group and a late-/post Caledonian displacement that cuts the Caledonian nappes has been reported earlier (Townsend et al., 1989; Siedlecka et al., 2011). The MSSZ must consequently represent a long-lived fault-zone (Olesen et al., 1992).

The Stuoragurra faulting has produced distinct deformation and fracturing of the host rock. Percussion and core drilling in the Fitnajohka area revealed a dip of c. 40° to the SE at a shallow depth of c. 100 m (Olesen et al., 1992, 2013; Roberts et al., 1997). The postglacial fault consists of zones of clay minerals, a few cm thick, within a 1.5 m thick interval of fractured quartzite. The clay zones contain kaolinite, vermiculite and smectite (Åm, 1994) and most likely represent a weathered fault gouge. Several 2–3 m thick zones of breccia occur within a 25 m wide interval and reveal that the postglacial faults were formed within an old zone of weakness partly coinciding with the margins of deformed Paleoproterozoic albite diabases.

The MSSZ terminates in the southwest against the Soagŋojávri-Bajášjávri Fault that constitutes the eastern fault of the regional Bothnian-Kvænangen Fault Complex (Berthelsen & Marker, 1986; Henkel, 1991; Olesen & Sandstad, 1993). The MSSZ can be traced on the aeromagnetic map below the Caledonian nappes, where the fault zone truncates the Levajok Granulite Belt below the Sværholt Peninsula (Olesen et al., 1990).

7. CONCLUSIONS

The two profiles depicted in the present report show that the snow-streamer technology is an efficient way to carry out seismic profiling in snow-covered and relatively flat terrain. Using a detonating cord as a seismic source has the clear advantage of leaving no permanent footprint on the sparse vegetation in the Arctic.

The regional c. 4-5 km wide Mierojávri-Sværholt shear zone is represented by several reflectors dipping at an angle of c. 40-50° to the southeast below the northwestern margin of the Jergul Gneiss Complex. The migrated seismic profile shows that the dip of the western and eastern segments of the postglacial Masi fault system (within the Stuoragurra fault complex) is 52° and 65°, respectively.

Eiken et al. (1989) and Johansen et al. (2011) have previously shown that the technique is applicable when mapping relatively flat-lying Mesozoic and Cenozoic sedimentary sequences on Svalbard. The present study shows that the technique can be applied to study Precambrian structures dipping at an angle of c. 45°. We think that much steeper structures would be difficult to image using the reflection seismic method.

Acknowledgements

The acquisition of the snow-streamer seismic profile in 2012 was funded by the Mineral Resources in North Norway (MINN) program initiated by the Norwegian government. Helge Johnsen at the University of Bergen was the leader for the field work during the acquisition of the snow-streamer seismic profile. Alf Kristian Nilsen, University of Oslo, Espen Lehn-Nilsen and Malin Waage, University of Bergen, Jomar Gellein and Geir Viken, NGU, Karstein Rød, Bergen Oilfield Services, Roar Helge Iversen, Dolphin Geophysical, Nils Per Nilsen Sara, Isak Anders Nilsen Eira, Klemet Anders Bals, Mikkel Per Bongo, Eskil Hermansen Hætta and Lars Johan Larsen Sara participated in the field campaign. Anne Liinamaa-Dehls improved the English text. We express our sincere thanks to all these persons for their contributions.

8. REFERENCES

Berthelsen, A. & Marker, M. 1986: 1.9-1.8 Ga old strike-slip megashears in the Baltic Shield, and their plate tectonic implications. In: Galson, D.A. & Mueller, S. (eds.), The European Geotraverse, Part 2. Tectonophysics, 128, 163-181.

Bingen, B., Solli, A., Viola, G., Torgersen, E., Sandstad, J.S., Whitehouse, M.J., Rohr, T.S., Ganerød, M. & Nasuti, A. 2015: Geochronology of the Palaeoproterozoic Kautokeino Greenstone Belt, Finnmark, Norway: Tectonic implications in a Fennoscandia context. Norwegian Journal of Geology, 95, 365–396. http://dx.doi.org/10.17850/njg95-3-09.

Chun, J.H. & Jacewitz, C.A. 1981: The first arrival time surface and estimation of statics: Presented at the 51st Annual Meeting of the Society of Exploration Geophysicists, Los Angeles.

Dalsegg, E. & Olesen, O. 2014: Resistivitetsmålinger ved Masi, Fitnajohka and Riednajávre og implikasjoner for malmleting. NGU Report 2014.021, 28 pp.

Dehls, J., Olesen, O., Olsen, L. & Blikra, L.H. 2000: Neotectonic faulting in northern Norway; the Stuoragurra and Nordmannvikdalen postglacial faults. Quaternary Science Reviews, 19, 1445-1460.

Eiken, O., Degutsch, M., Riste, P. & Rød, K. 1989: Snowstreamer: an efficient tool in seismic acquisition. First Break, 7(9), 374-378.

Fundal, E. 1967. En undersøkelse i det prekambriske Biggevarre område i Finnmark, Nord-Norge med særlig henblikk på de såkalde albitdiabasers geologi og petrografi. NGU Report 680, 81 pp.

Henderson, I.H.C., Viola, G. & Nasuti, A. 2015. A new tectonic model for the Kautokeino Greenstone Belt, northern Norway, based on high resolution airborne magnetic data and field structural analysis and implications for mineral potential. Norwegian Journal of Geology 95, 339–363. http://dx.doi.org/10.17850/njg95-3-05

Henkel, H. 1991. Magnetic crustal structures in northern Fennoscandia. In P. Wasilewski, P. Hood, (eds.), Magnetic anomalies – land and sea. Tectonophysics 192, pp. 57-79.

Henriksen, H. 1986. Bedrock map Iddjajavri 2034 II M 1:50 000, preliminary edition. Geological Survey of Norway.

Johansen, T.A., Ruud, B.O., Bakke, N.E., Riste, P., Johannessen, E., & Henningsen, T. 2011. Seismic profiling on Arctic glaciers. First Break, 29(2), 29-35.

Korenaga, J., Holbrook, W.S., Kent, G.M., Kelemen, P.B., Detrick, R.S., Larsen, H.-C., Hopper, J.H. & Dahl-Jensen, T. 2000: Crustal structure of southeast Greenland margin from joint reflection and refraction tomography. Journal of Geophysical Research, 105 (B9), 21591-21614.

Lagerbäck, R. & Sundh, M. 2008. Early Holocene faulting and paleoseismicity in northern Sweden. Sver. Geol. Unders., C836, 80 pp.

Mrope, F.M., Becken, M., Ruud, B.O., Olesen, O., Johansen, T.A., Brönner, M., Gradmann, S. & Nasuti, A. 2019. Magnetotelluric 2D inversion and joint interpretation of MT, seismic, magnetic and gravity data from Masi, Kautokeino municipality, Finnmark. NGU Report, 2019.009, 64 pp.

Nasuti, A., Roberts, D., Dumais, M.-A., Ofstad, F., Hyvönen, E., Stampolidis, A. & Rodionov, A. 2015. New high-resolution aeromagnetic and radiometric surveys in Finnmark and North Troms: linking anomaly patterns to bedrock geology and structure. Norwegian Journal of Geology, 95, 217–243. http://dx.doi.org/10.17850/njg95-3-10.

Olesen, O. 1988. The Stuoragurra Fault, evidence of neotectonics in the Precambrian of Finnmark, northern Norway. Norsk Geologisk Tidsskrift, 68, 107-118.

Olesen, O. & Sandstad, J. 1993. Interpretation of the Proterozoic Kautokeino Greenstone Belt, Finnmark, Norway from combined geophysical and geological data. Geological Survey of Norway Bulletin, 425, 43–64.

Olesen, O., Roberts, D., Henkel, H., Lile, O.B. & Torsvik, T.H. 1990. Aeromagnetic and gravimetric interpretation of regional structural features in the Caledonides of West Finnmark and Northern Troms, north Norway. Geological Survey of Norway Bulletin, 419, 1–24.

Olesen, O., Henkel, H., Lile, O.B., Mauring, E. & Rønning, J.S. 1992. Geophysical investigations of the Stuoragurra postglacial fault, Finnmark, northern Norway. Journal of Applied Geophysics, 29, 95–118.

Olesen, O., Bungum, H., Lindholm, C., Olsen, L., Pascal, C. & Roberts, D. 2013. Neotectonics, seismicity and contemporary stress field in Norway – mechanisms and implications. In L. Olsen, O. Fredin, O. Olesen (eds.) Quaternary Geology of Norway. Geological Survey of Norway Special Publication, 13, 145-174.

Olesen, O., Olsen, L., Gibbons, S., Ruud, B.O., Høgaas, F., Johansen, T.A. & Kværna, T. in press. Postglacial faulting in Norway - Large magnitude earthquakes of late Holocene age. In: H. Steffen, O. Olesen, and R. Sutinen, eds, Glacially Triggered Faulting, Cambridge University Press.

Olsen, L., Olesen, O. & Høgaas, F. 2021: A part of the Stuoragurra postglacial fault complex, at Máze in N-Norway, is less than 600 yrs old. Vinterkonferansen 2021, Digital, January 6th-8th, 2020, H.A. Nakrem & A.M. Husås (eds.), Abstracts and Proceedings of the Geological Society of Norway No. 1, 2021, p 55.

Roberts, D., Olesen, O. & Karpuz, M.R. 1997: Seismo- and neotectonics in Finnmark, Kola Peninsula and the southern Barents Sea; Part 1, Geological and neotectonic framework. Tectonophysics, 270, 1-13.

Russell, B.H. 1989: Statics Corrections — A Tutorial. CSEG Recorder, 14, 16–30.

Rygg, E., Riste, P., Nøttvedt, A., Rød, K. & Kristoffersen, Y. 1992: The snowstreamer – a new device for acquisition of seismic data on land. In: T.O. Vorren, E. Bergsaker, Ø.A. Dahl-Stamnes, E. Holter, B. Johansen, E. Lie and T.B. Lund

(eds.) Arctic Geology and Petroleum Potential. NPF Special Publications 2, pp. 703-709, Elsevier, Amsterdam.
Siedlecka, A. 1985. Geology of the Iešjávri-Skoganvarre area, northern Finnmarksvidda, North Norway. Geological Survey of Norway Bulletin, 403, 103112.
Siedlecka, A. 1987. Berggrunnskart Iešjávri; 1934 II, foreløpig utgave, M 1:50 000. Norges geologiske undersøkelse, Trondheim.
Siedlecka, A. & Roberts, D. 1996. Finnmark Fylke. Berggrunnsgeologi M 1:500 000. Norges geologiske undersøkelse, Trondheim.
Siedlecka, A., Davidsen, B., Rice, A.H.N. & Townsend, C. 2011. Berggrunnskart; Skoganvarri 2034 IV, M 1:50 000, revidert foreløpig utgave. Norges geologiske undersøkelse, Trondheim.
Solli, A. 1983. Precambrian stratigraphy in the Masi area, Southwestern Finnmark, Norway. Geological Survey of Norway Bulletin, 380, 97-105.
Solli, A. 1988. Masi, 1933 IV - berggrunnsgeologisk kart - M 1:50,000. Nor. geol. unders., Trondheim.
Townsend, C., Rice, A.H.N. & Mackay, A. 1989. The structure and stratigraphy of the southwestern portion of the Gaissa Thrust Belt and the adjacent Kalak Nappe Complex, N Norway. In R.A. Gayer (Ed.) The Caledonide Geology of Scandinavia. Graham and Trotman, London, 111-126.
Zwaan, K.B. 1985. Berggrunnskart Suolovuopmi 1934 III, M 1:50 000, foreløpig utgave. Norges geologiske undersøkelse, Trondheim.
Åm, M. (1994). Mineralogisk og petrologisk karakterisering av vitrings/sleppemateriale fra Stuoragurraforkastningen, Finnmark. MSc thesis, Norwegian University of Science and Technology, 102 pp.

Figure 1. Pictures from the field work. a) From the western line at Sennalandet. b) From the western line at Masi. c) Working with the snowstreamer at the drum. d) Node for recording. e) and f) Shots made with detonating cord.

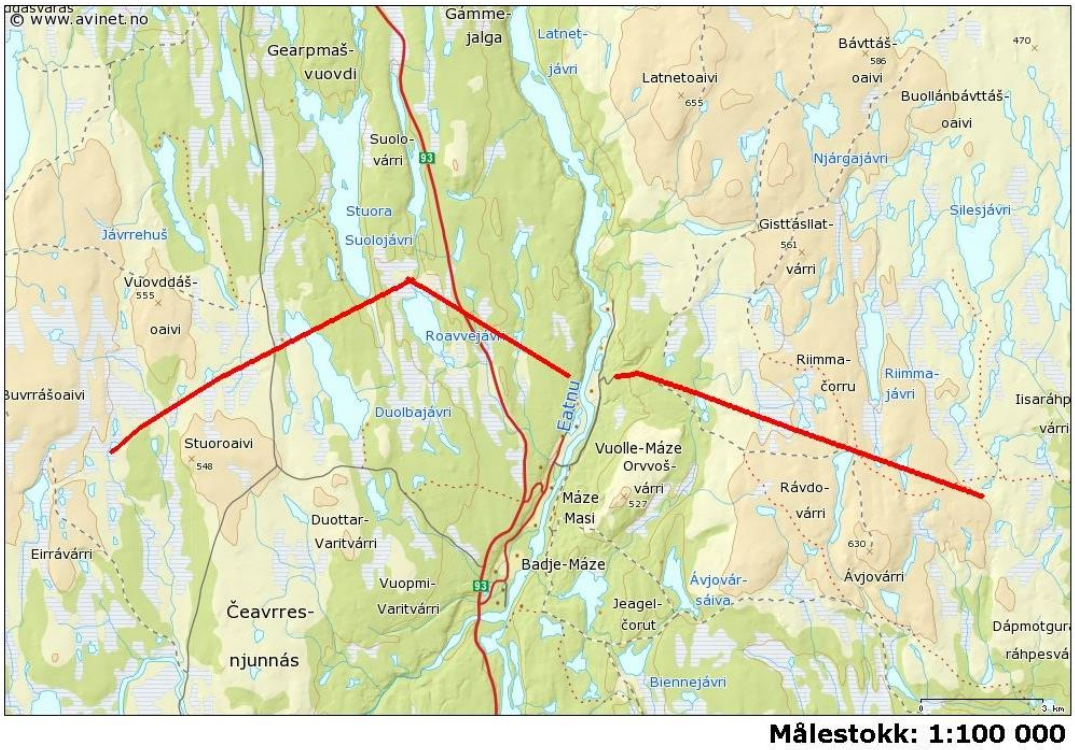

Figure 2. Map with the seismic profile consisting of three lines near Masi. The western and central lines have different orientations. They are connected at the breakpoint north of lake Roavvejávri. Note that the western line has two small kinks. The gap between the central and eastern lines are caused by the Kautokeino River and the adjacent steep slopes.

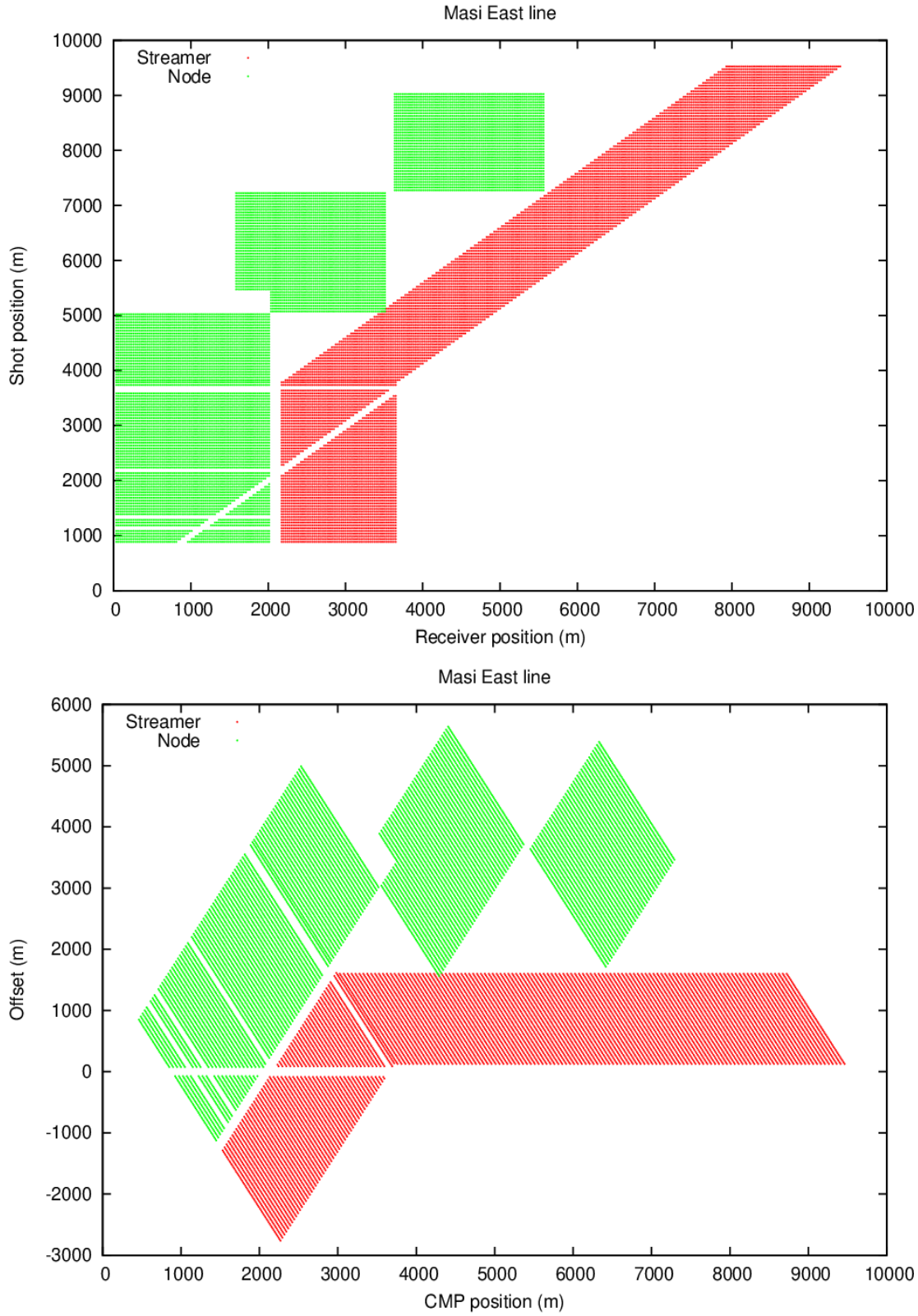

Figure 3. Masi eastern line was shot from the west towards the east and was recorded with both snow-streamer (red dots, may not be resolvable) and nodes (green dots, may not be resolvable). The upper figure (a) shows the positions of receivers and sources (shots). Lower figure (b) shows how the recorded traces are distributed in CMP (common midpoint) position and offset.

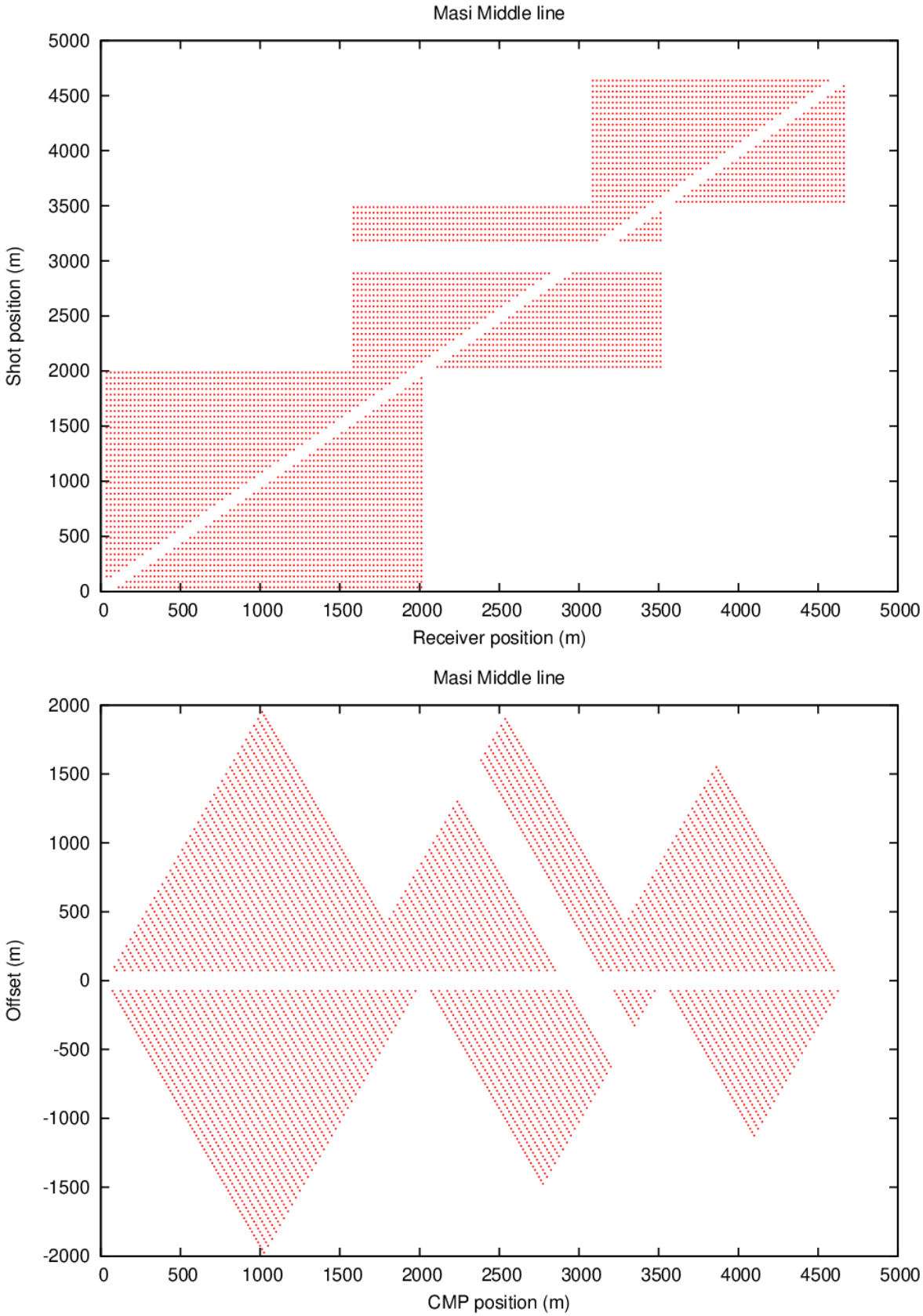

Figure 4. Masi middle line was shot from the east towards the west and was recorded with nodes only. The upper figure (a) shows the positions of receivers and sources (shots). Lower figure (b) shows how the recorded traces are distributed in CMP (common mid-point) position and offset.

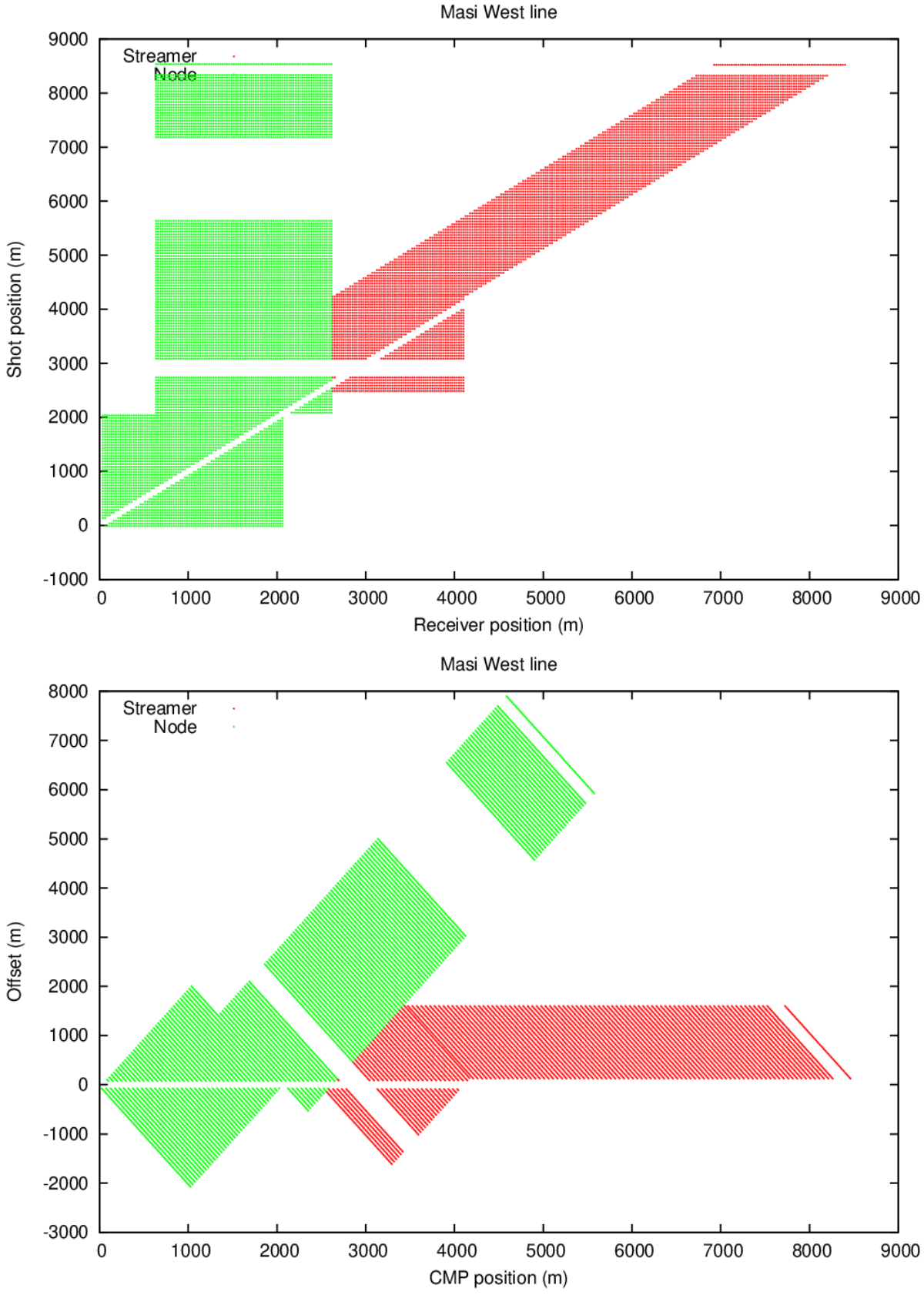

Figure 5. Masi western line was shot from the east towards the west and was recorded with both snow-streamer (red dots, may not be resolvable) and nodes (green dots, may not be resolvable). The upper figure (a) shows the positions of receivers and sources (shots). Lower figure (b) shows how the recorded traces are distributed in CMP (common mid-point) position and offset.

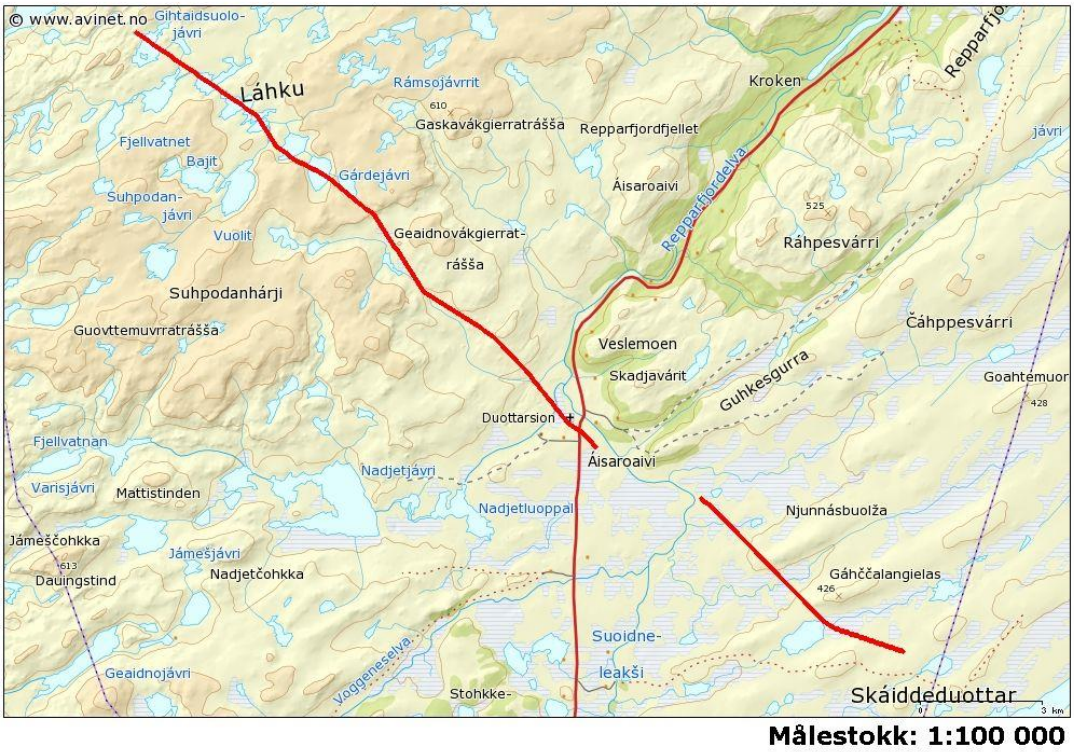

Figure 6. Map with the profile consisting of two lines at Sennalandet. The gap between the two lines to the east of Áisaroaivi is caused by the high-voltage power line. It is not allowed to use explosives with electrical ignition in this area.

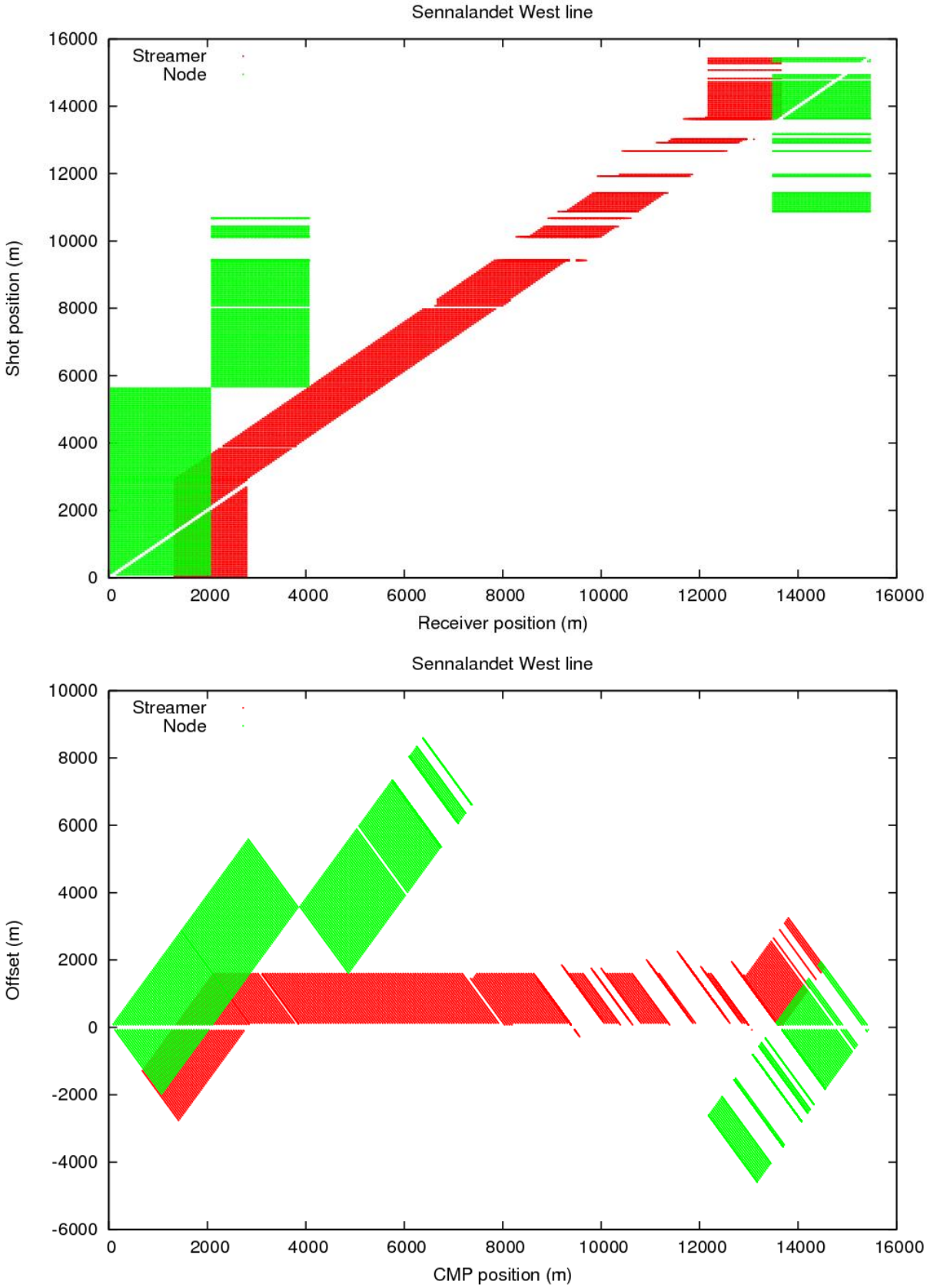

Figure 7. Sennalandet western line was shot from the east towards the west and was recorded with both snow-streamer (red dots, irresolvable) and nodes (green dots, irresolvable). The upper figure (a) shows positions of receivers and sources (shots). Lower figure (b) shows how the recorded traces are distributed in CMP (common midpoint) position and offset.

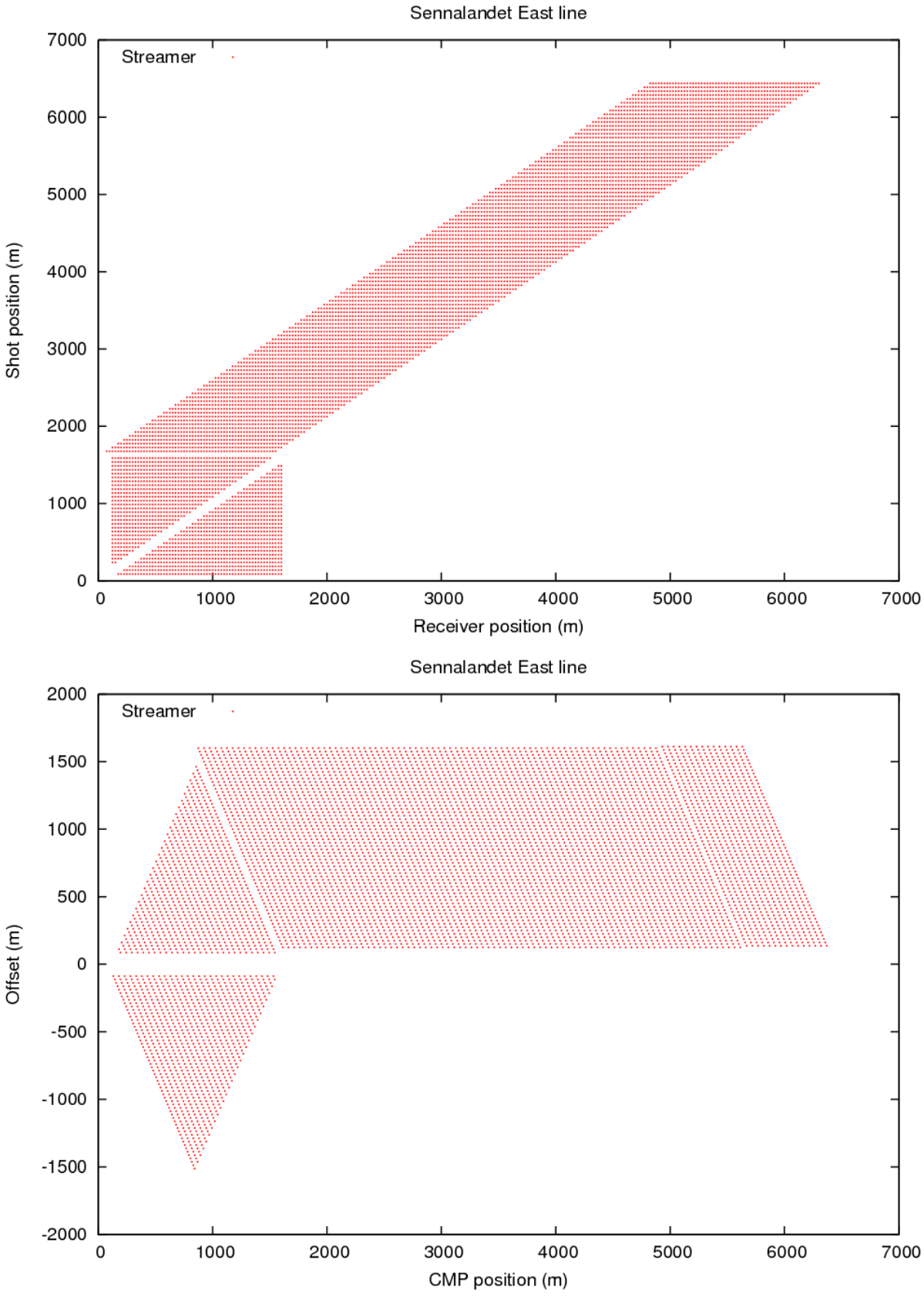

Figure 8. Sennalandet eastern line was shot from the west towards the east and was recorded with snow-streamer only. The upper figure (a) shows positions of receivers and sources (shots). Lower figure (b) shows how the recorded traces are distributed in CMP (common mid-point) position and offset.

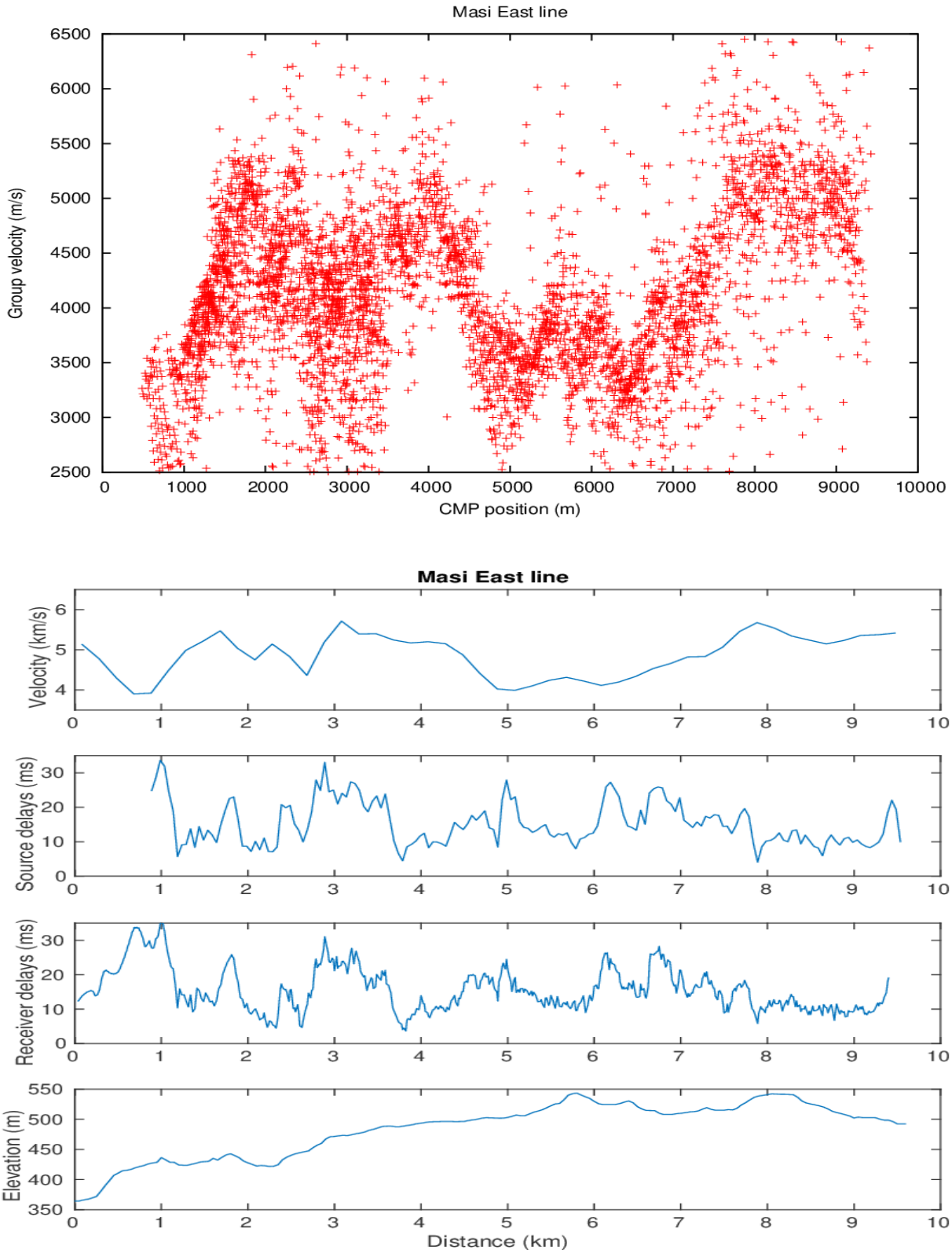

Figure 9. Above (a): Group velocity (offset divided by travel-time) from automatically picked first arrivals in the offset interval 100-1000 m. Below (b): Refraction velocities and time delays (statics) derived from the first breaks showed above.

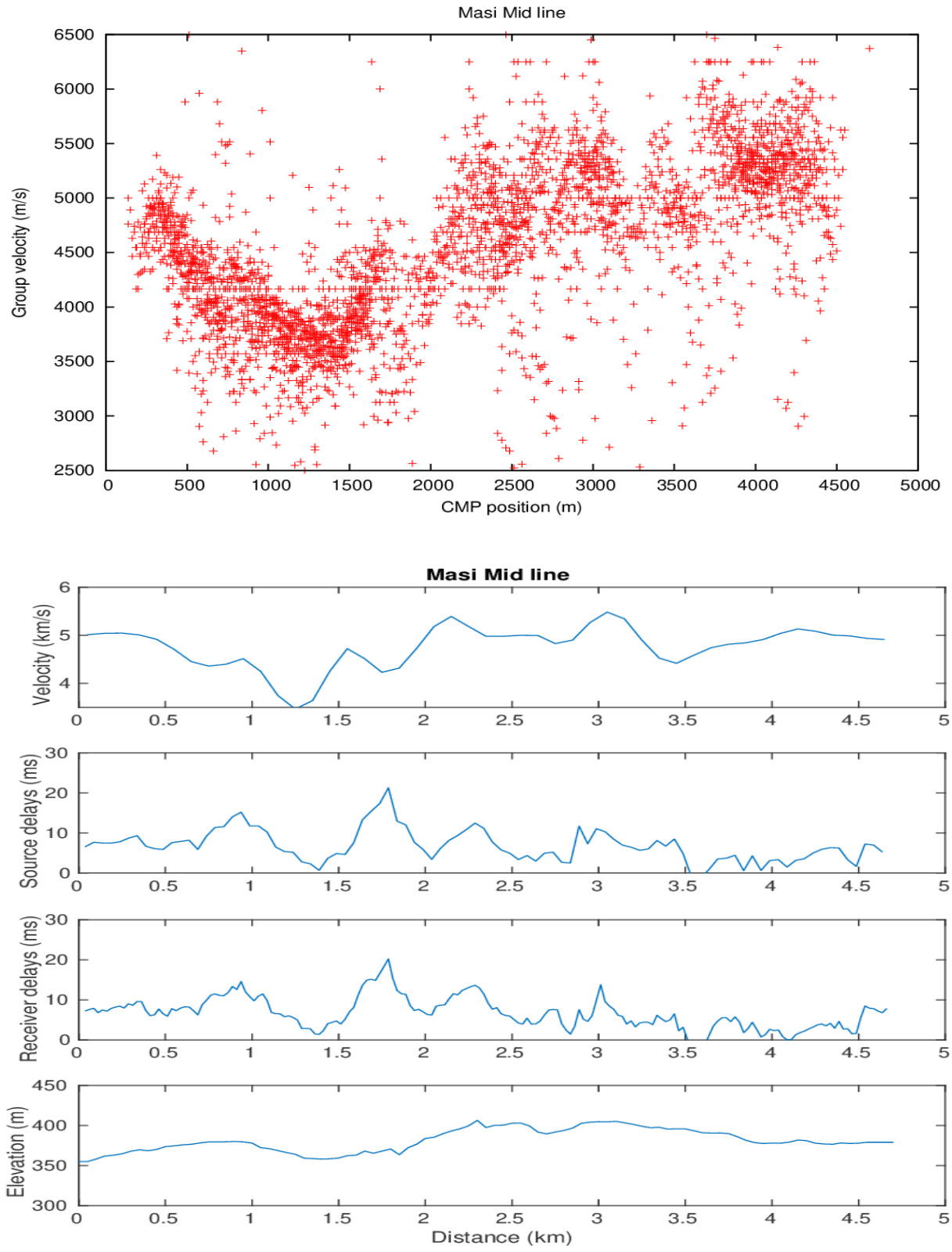

Figure 10. Above (a): Group velocity (offset divided by travel-time) from automatically picked first arrivals in the offset interval 100-1000 m. Below (b): Refraction velocities and time delays (statics) derived from the first breaks showed above.

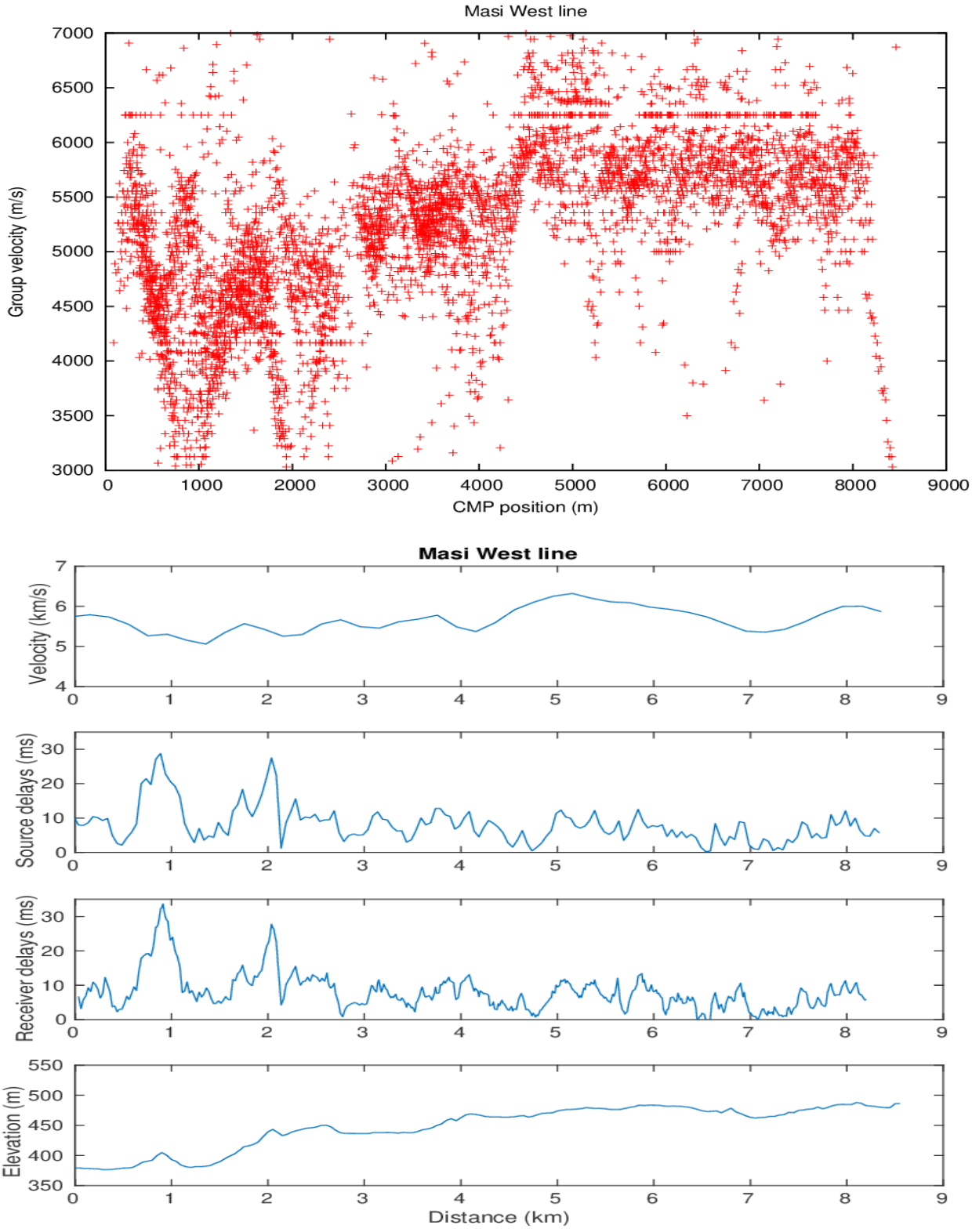

Figure 11. Above (a): Group velocity (offset divided by travel-time) from automatically picked first arrivals in the offset interval 100-1000 m. Below (b): Refraction velocities and time delays (statics) derived from the first breaks showed above.

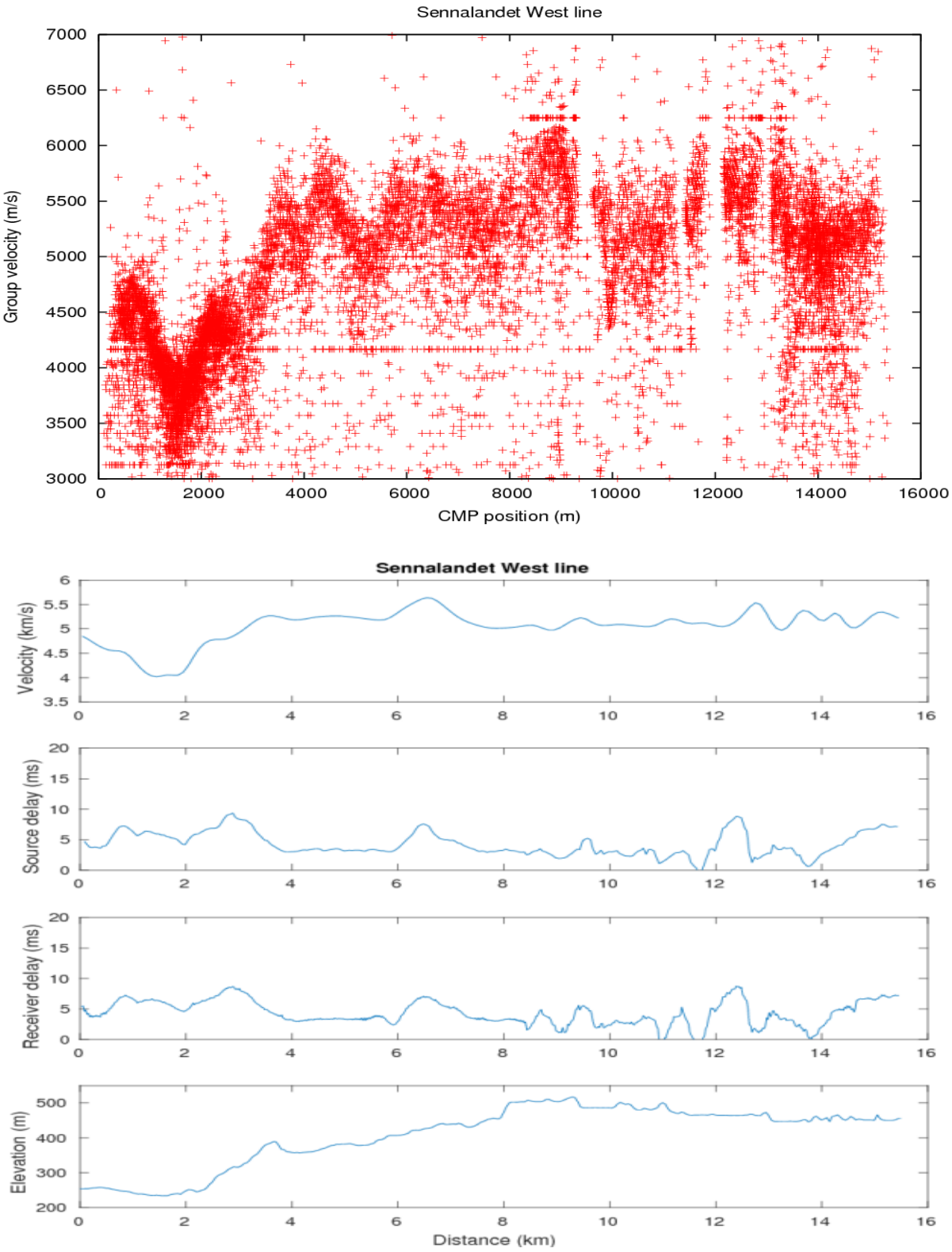

Figure 12. Above (a): Group velocity (offset divided by travel-time) from automatically picked first arrivals in the offset interval 100-1000 m. Below (b): Refraction velocities and time delays (statics) derived from the first breaks showed above.

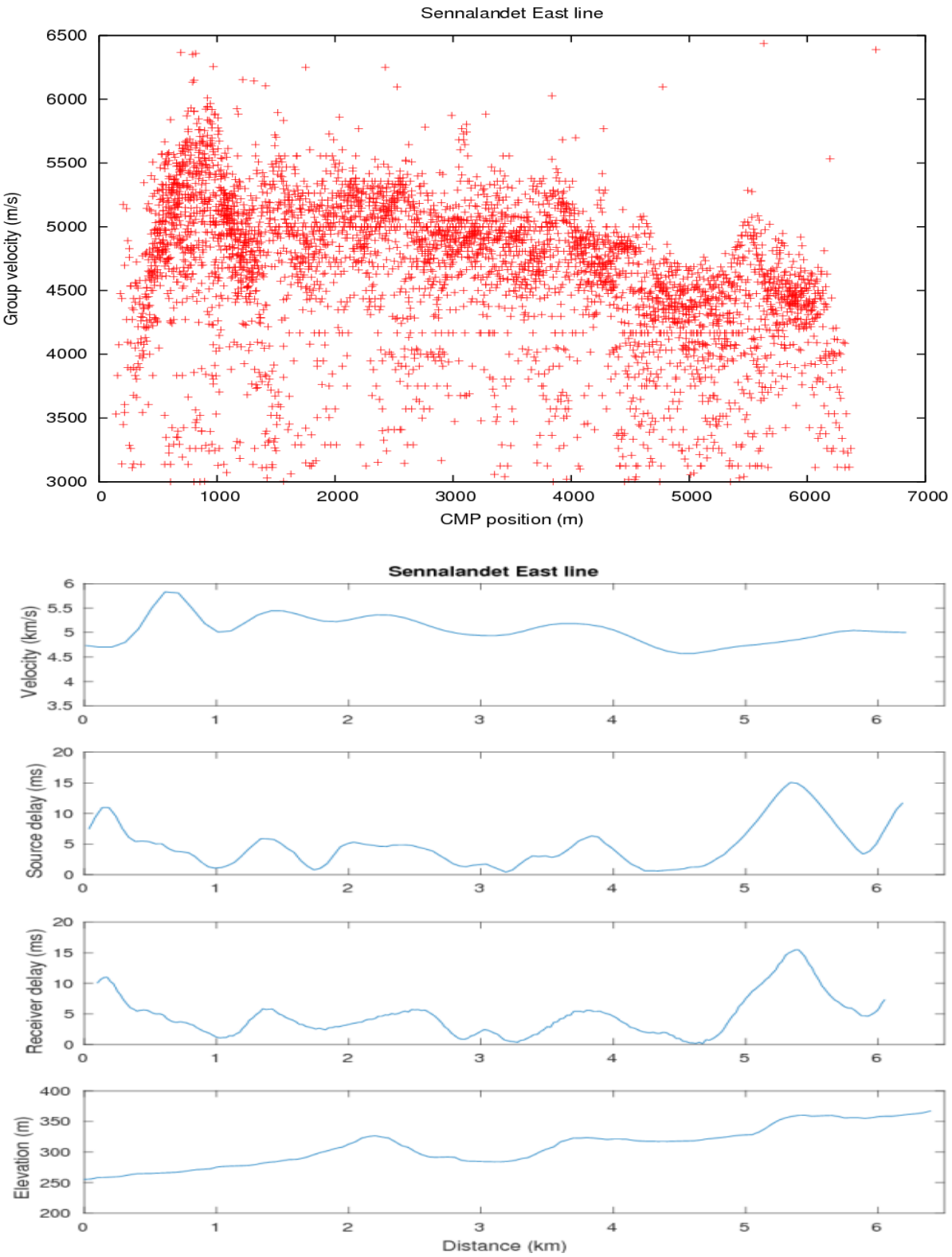

Figure 13. Above (a): Group velocity (offset divided by travel-time) from automatically picked first arrivals in the offset interval 100-1000 m. Below (b): Refraction velocities and time delays (statics) derived from the first breaks showed above.

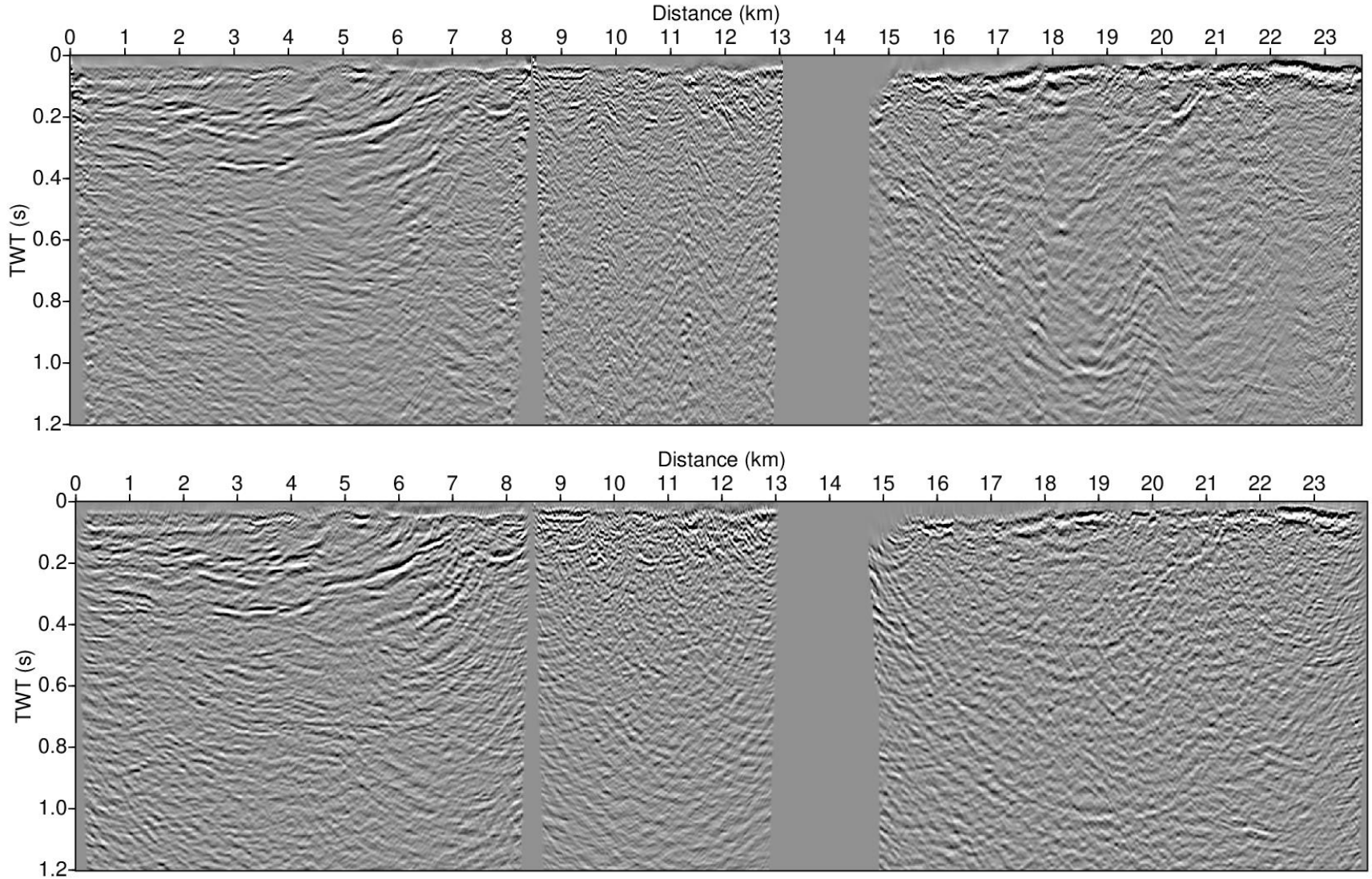

Figure 14. Seismic sections composed of the three lines near Masi displayed from the west towards the east. Above (a) Stack after DMO. Below (b) Migrated stack.

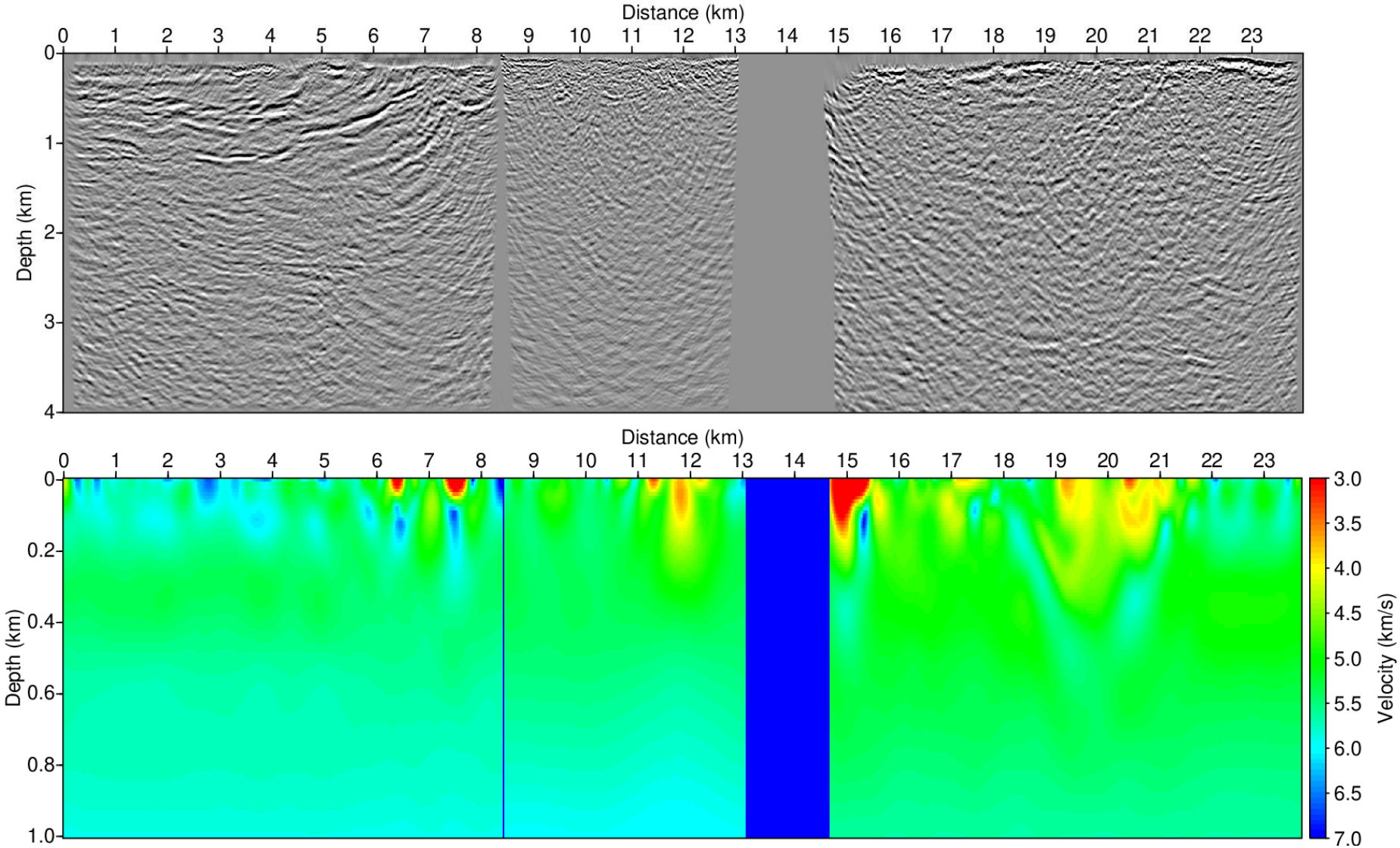

Figure 15. Seismic sections composed of the three lines near Masi. Above (a): Depth converted migrated stack. Below (b): P-wave velocities obtained from travel-time tomography of manually picked first breaks.

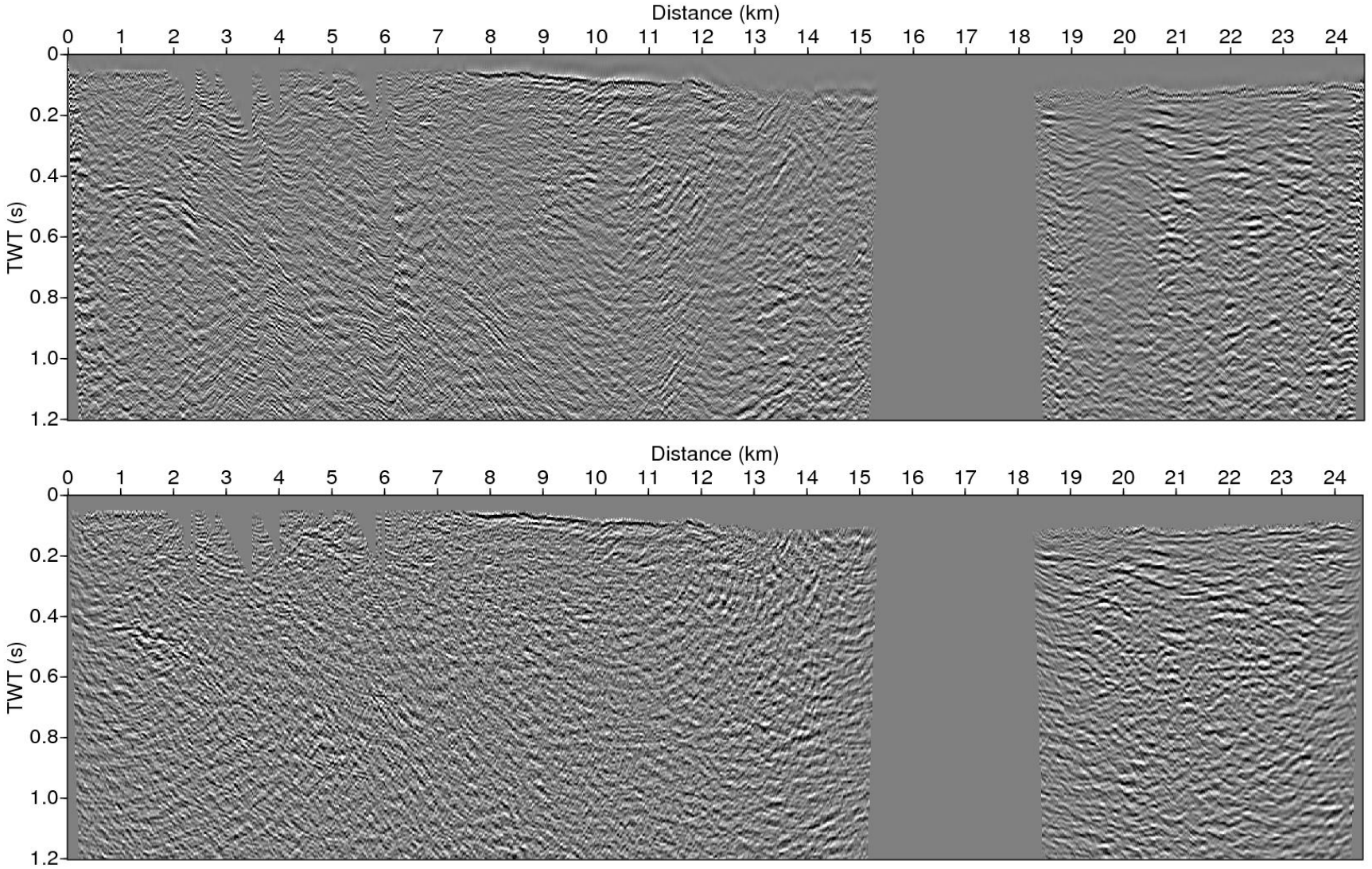

Figure 16. Seismic sections composed of the two lines at Sennalandet, displayed from the west towards the east. Above (a) Stack after DMO. Below (b) Migrated stack.

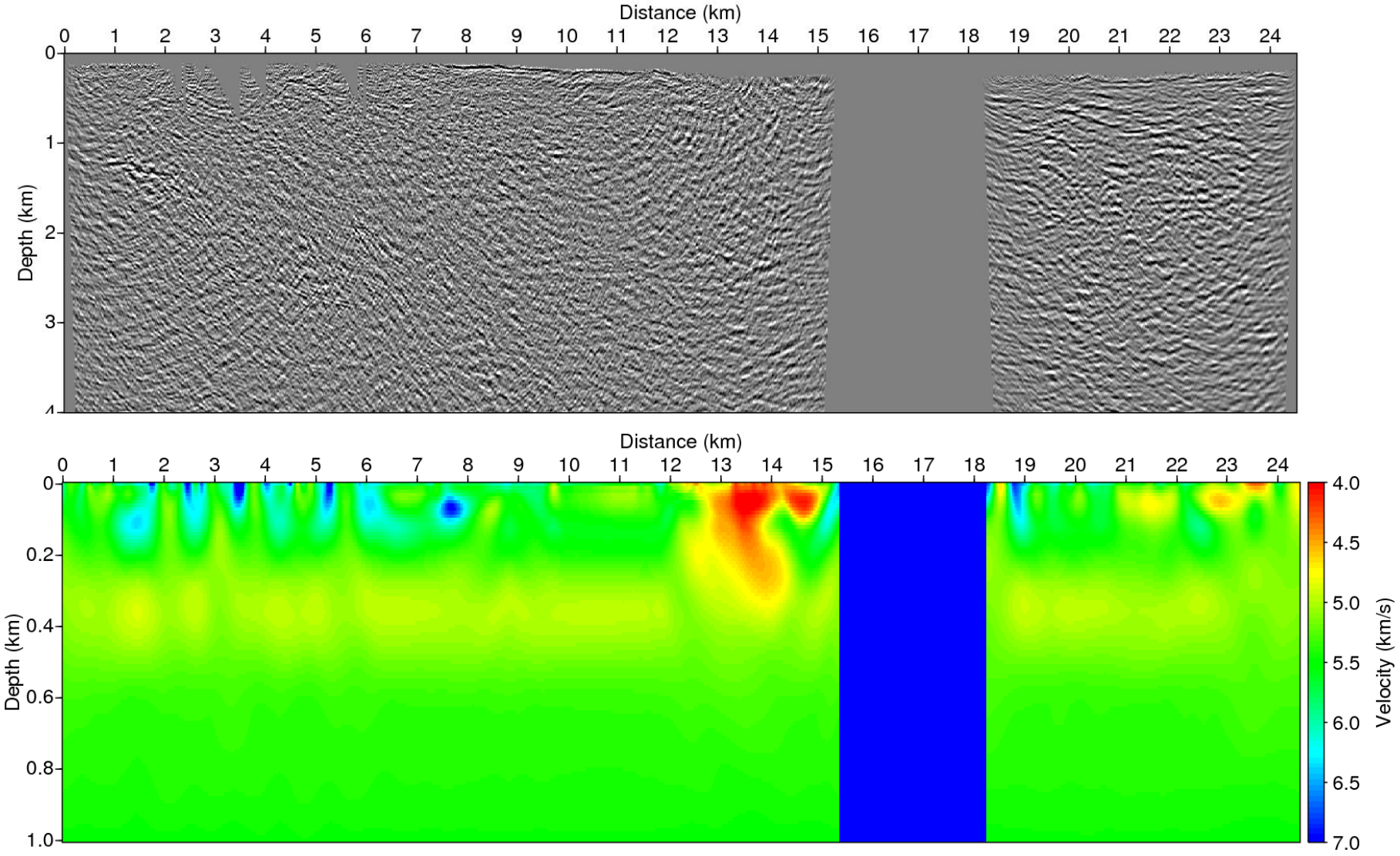

Figure 17. Seismic sections composed of the two lines at Sennalandet. Above (a): Depth converted migrated stack. Below (b): P-wave velocities obtained from travel-time tomography of manually picked first breaks.

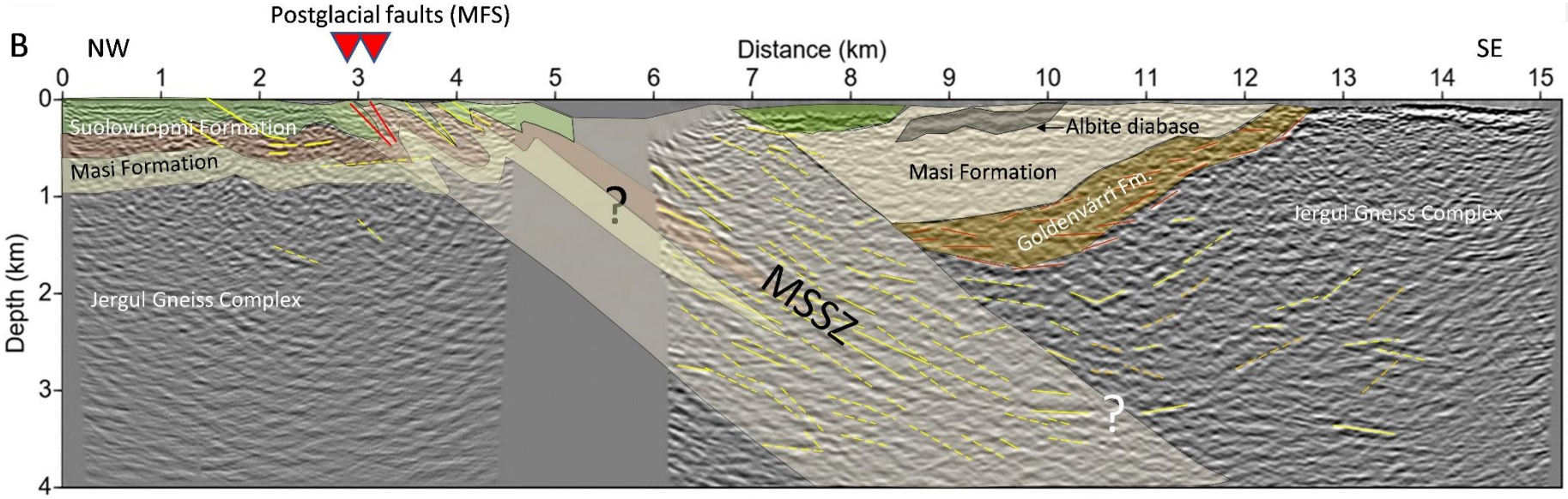

Figure 18. Interpretation of the migrated and depth-converted version of the two easternmost lines shown in Figure 15. The MSSZ and SFC/MFS are shown by the pale grey raster and two red lines, respectively. The interpretation is partly based on earlier geological and geophysical studies (Olesen, 1988; Solli, 1988; Olesen et al., 1992; Henderson et al. 2015; Mrope et al. 2019). The seismic profile cuts the MFS and MSSZ at an angle of 70°. The apparent dip of the MSSZ is c. 40° to the SE. A correction for the oblique crossing of the MSSZ increases the dip angle to 43°. The MFS is located within the regional c. 4 km wide MSSZ. The dips of the western and eastern segments of the MFS within the SFC as read from the migrated seismic section are 48° and 59°, respectively. The dip increases to 52° and 65° after correcting for oblique crossing. The two postglacial fault segments seem to merge at a depth of c. 500 m. The postglacial faults are partly parallel to the axial plane of the folds along the MSSZ (Olesen et al. 1992; Roberts et al., 1997). The flat-lying reflector along the southeastern margin of the MSSZ at a depth of 3-4 km may represent a tectonic ramp associated with a phase of thrusting or detachment faulting along the fault zone.

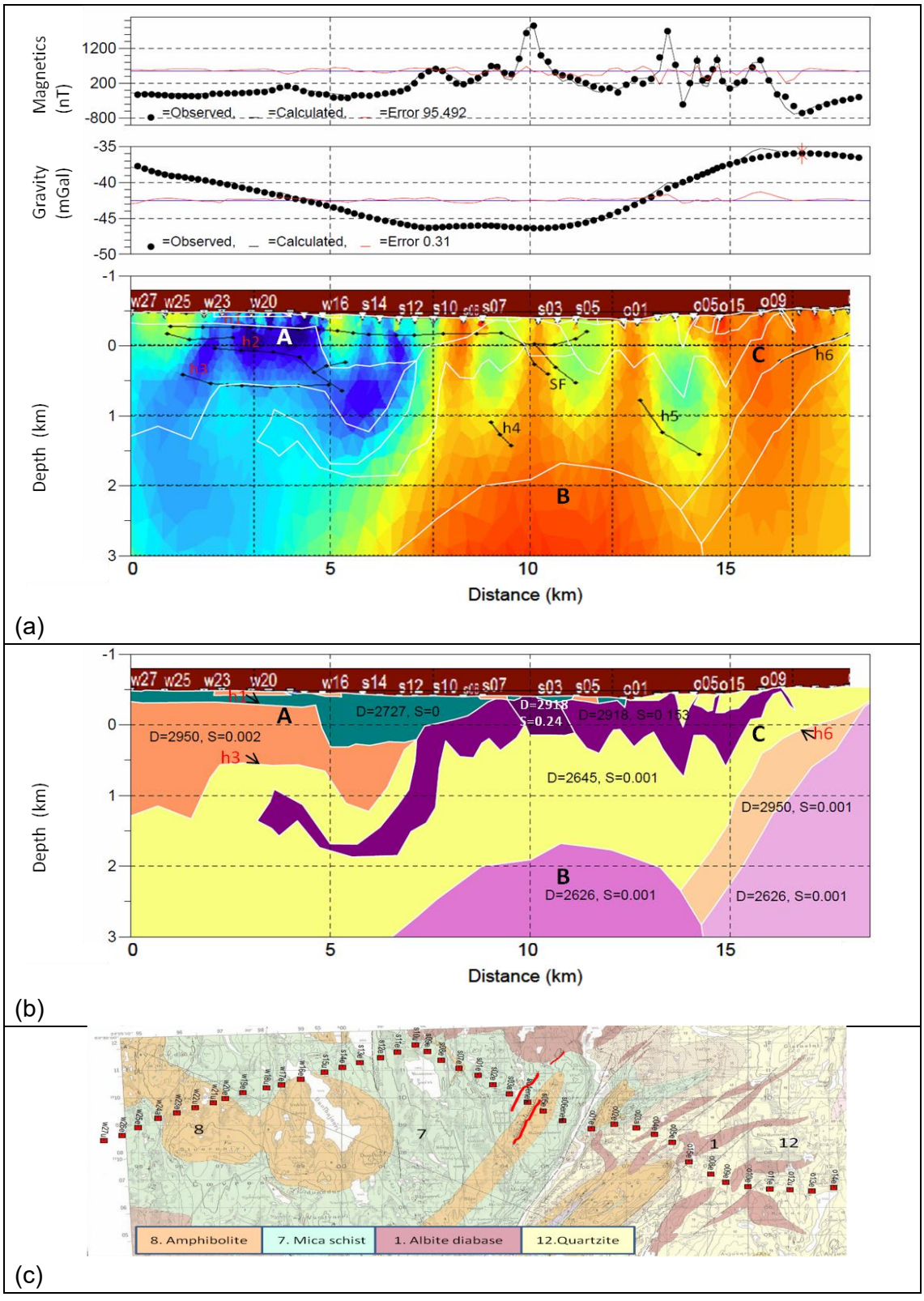

Figure 19. (a) Magnetics and gravity data (top panels) jointly interpreted with MT resistivity model and seismic reflectors, h1-h6, SFC (Mrope et al., 2019). (b) The interpreted geological model is based on the MT resistivity boundaries, seismic reflectors. (c) Geological map to demarcate the density and susceptibility zones to fit the observed gravity and magnetic data respectively along the profile. The difference (red lines) between the observed data (solid circles) and the calculated (black lines) is relatively small. The RMS error is 95.492 for magnetic and 0.310 for gravity data.

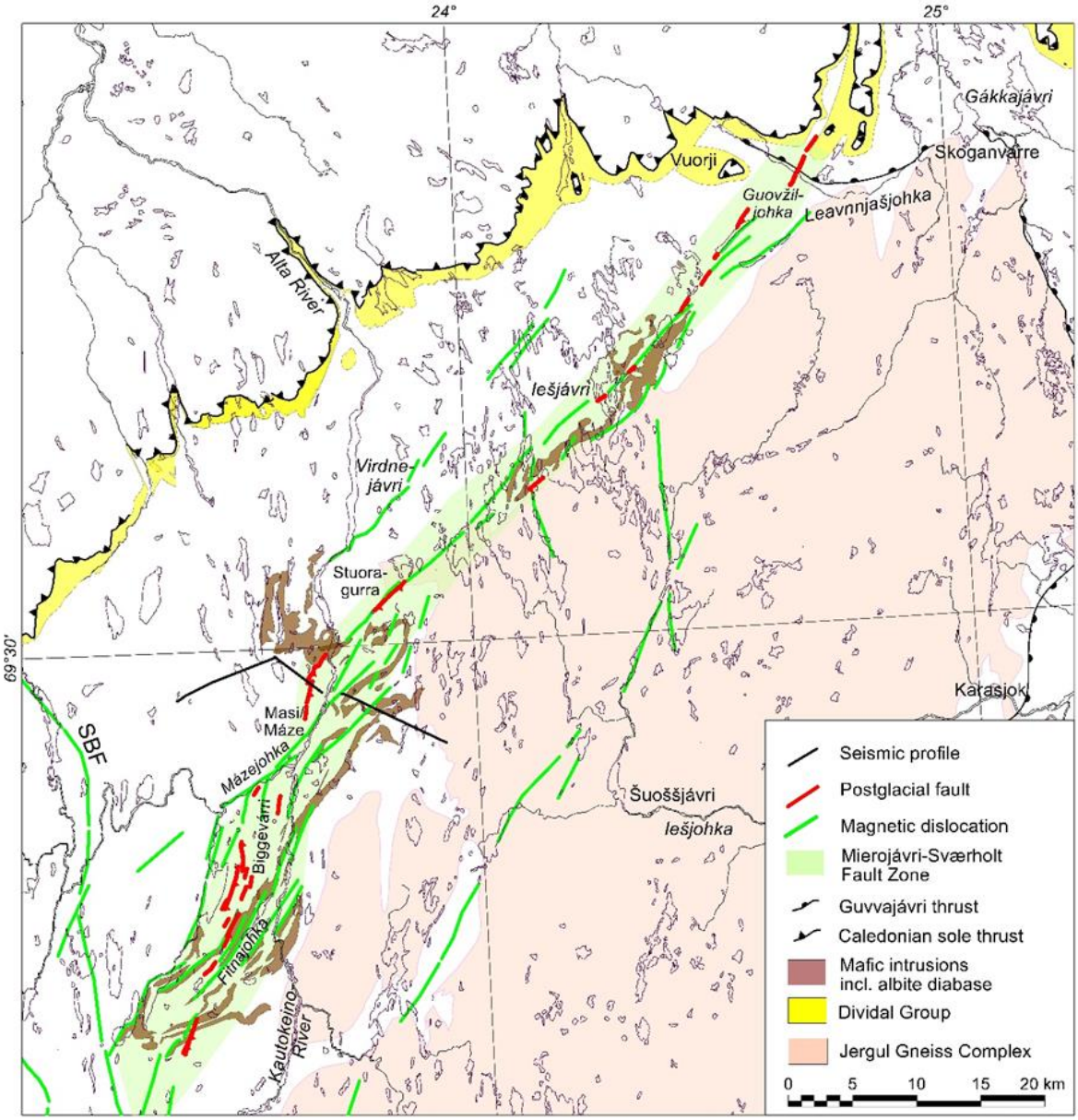

Figure 20. Simplified geological map of Finnmarksvidda (from Zwaan, 1985; Henriksen, 1986; Siedlecka, 1987; Solli, 1988; Olesen & Sandstad, 1993; Siedlecka & Roberts, 1996; Siedlecka et al., 2011). The 4-5 km wide Mierojávri-Sværholt shear zone (MSSZ) is located along the northwestern boundary of the Jergul Gneiss Complex (Olesen et al., 1992). The MSSZ is also characterized by magnetic anomalies produced by the highly magnetic mafic intrusions (diabase, albite diabase and gabbro). An albite diabase south of Masi has been dated by Bingen et al. (2015) to 2220 ± 7 Ma. The mafic intrusions are partly adapted from the 1:50 000 bedrock maps (Fundal, 1967; Zwaan, 1985; Solli, 1988; Siedlecka, 1987) and partly interpreted from aeromagnetic maps (Nasuti et al., 2015). The postglacial faults are adapted from Olesen et al. (in press). The 90 km long Stuoragurra fault complex (SFC) consists of three separate fault systems; the Fitnajohka fault system in the southwest, the Máze fault system in the central area and the Iešjávri fault system to the northeast. The SFC occurs within the MSSZ. SBF – Soagŋojávri-Bajášjávri Fault (Olesen & Sandstad, 1993).

Appendix I: Procedure for static corrections

A well-known method used for computing surface consistent refraction statics is the time-term method (Russell, 1989; Chun & Jacewitz, 1981). In this method it is assumed that the refraction velocity is constant, which is obviously not the case for much of our data where the lines cross over the boundary between the sediment basin and the basement rock. To account for the lateral velocity variations, we computed the travel-time of the first arrival as:

$$T_{ij} = \int_{Xi}^{Xj} \frac{dx}{v(x)} + t_S(x_i) + t_R(x_j)$$

where T_{ij} is the travel-time from source i to receiver j, x_i is the source position, x_j is the receiver position, v(x) is the laterally varying refraction velocity, $t_s(x_i)$ is the time delay of the source, and $t_r(x_j)$ is the time delay of the receiver. If v(x) is constant, this equation reduces to that of the original time-term method. A piecewise linear function for v(x) was used with 150 m between the velocity nodes. Since the contribution of the horizontal part of the ray to the travel-time is an integral over the inverse velocity, the travel-time will be smooth functions of the horizontal coordinate. More irregular variations in the travel-time must be accounted for by the time-terms. An automatic first break picker was used to pick arrival times within a guided time window. This resulted in thousands of travel-times for each line, which were then used to compute the hundreds of unknowns (velocities and time-terms) in a damped linear inversion.

Appendix II: Seimic archive data

(in SEG-Y format and stored in the NGU ground geophysics database)

```
Raw data files:
     Line-1-snowstreamer.segy - East Line Masi
     Line-1-nodes.segy - East Line Masi
     Line-2-nodes-segy - Mid Line Masi
     Line-3-snowstreamer.segy - West Line Masi
     Line-3-nodes.segy - West Line Masi
     Line-4-snowstreamer.segy - West Line Sennalandet
     Line-4-nodes.segy - West Line Sennalandet
     Line-5-snowstreamer.segy - East Line Sennalandet

Processed data:
  Stack after DMO:
     Line-1-stack.segy – East Line Masi
     Line-2-stack.segy – Mid Line Masi
     Line-3-stack.segy – West Line Masi
     Line-4-stack.segy – West Line Sennalandet
     Line-5-stack.segy – East Line Sennalandet

  Migrated DMO corrected stack:
     Line-1-mig.segy – East Line Masi
     Line-2-mig.segy – Mid Line Masi
     Line-3-mig.segy – West Line Masi
     Line-4-mig.segy – West Line Sennalandet
     Line-5-mig.segy – East Line Sennalandet

  Depth converted migrated DMO stack:
     Line-1-depth.segy – East Line Masi
     Line-2-depth.segy – Mid Line Masi
     Line-3-depth.segy – West Line Masi
     Line-4-depth.segy – West Line Sennalandet
     Line-5-depth.segy – East Line Sennalande

Files with shot point coordinates (UTM zone 33W, ASCII text):
     Line-1-Masi-East.txt
     Line-2-Masi-Mid.txt
     Line-3-Masi-West.txt
     Line-4-Sennalandet-West.txt
     Line-5-Sennalandet-East.txt
```

Specifications for the SEG-Y files

Raw data:

Sources: 2 parallel detonating cords (with 40 g/m PETN) 50 meters long. Shot interval: 50 m.

Receivers: strings of 8 vertical geophones (SM-4, 14 Hz), half-gimballed in cylindrical metal cases, coupled in series, equidistant distributed over 25 m group length. Group interval: 25 m.

Recording: Geometrics Geode for the snowstreamer, and Sercel Unite RAU3 nodes. In both cases the sampling interval is 2 ms and the recording length is 6000 ms (3000 samples per trace).

Trace headers:
Byte
9 – 12: field record number (different for snowstreamer and nodes)
13 – 16: trace number on the spread
17 – 20: shot point number
21 – 24: CMP number (Common Mid Point)
37 – 40: signed offset (m) (shot position minus receiver position)
41 – 44: surface elevation at receiver (masl)
45 – 48: surface elevation at source (masl)
73 – 76: source position (m) (distance along line)
81 – 84: receiver position (m) (distance along line)

Shot point numbers start around 101 for each line. Distances along the line are computed as the shot point number multiplied by the shot interval (50 m). When shooting at shot point N, the detonating cord lays between shot point N-1 and N. Source and receiver positions refer to the midpoints of the sources and receivers. CMP numbers are computed as the CMP position divided by the CMP interval (12.5 m). Shot point coordinates (UTM 33W) are stored in separate text files.

Processed data:

The files contain CMP traces with an interval of 12.5 m. The CMP numbers are 4 times larger than the shotpoint number in the same position. Thus the CMP numbers start around 400 for each line.

Trace headers:
Byte
9 – 12: shot point number nearest to the current CMP
45 – 48: surface elevation at the CMP (masl)
73 – 76: CMP east coordinate (UTM 33W)
77 – 80: CMP north coordinate (UTM 33W)
115 – 116: number of samples in trace
117 – 118: sampling interval (microseconds for time, meters for depth converted data)

GEOLOGICAL
SURVEY OF
NORWAY

· NGU ·

Geological Survey of Norway
PO Box 6315, Sluppen
N-7491 Trondheim, Norway

Visitor address
Leiv Eirikssons vei 39
7040 Trondheim

Tel (+ 47) 73 90 40 00
E-mail ngu@ngu.no
Web www.ngu.no/en-gb/